ESKİŞEHİR TECHNICAL UNIVERSITY JOURNAL OF SCIENCE AND TECHNOLOGY
A- APPLIED SCIENCES AND ENGINEERING

Estuscience – Se, 2024, 25 [3] pp. 390-406, DOI: 10.18038/estubtda.1432952

RESEARCH ARTICLE

DETERMINATION OF DEEP RED REMOVAL POTENTIAL OF ACTIVATED CARBON PRODUCED FROM WHEAT BRAN

Ilknur DEMIRAL [1], Canan SAMDAN [2,*], Fatma Betül KUS [3]

[1] Eskişehir Osmangazi University, Faculty of Engineering and Architecture, Department of Chemical Engineering, 26480 Eskişehir, Turkey
idemiral@ogu.edu.tr - 0000-0003-2867-5205

[2] Eskişehir Osmangazi University, Faculty of Engineering and Architecture, Department of Chemical Engineering, 26480 Eskişehir, Turkey
caydin@ogu.edu.tr - 0000-0001-8755-0790

[3] Eskişehir Osmangazi University, Faculty of Engineering and Architecture, Department of Chemical Engineering, 26480 Eskişehir, Turkey
ftmbtl341016@hotmail.com - 0000-0003-4223-4596

Abstract

In this study, the production of activated carbon from wheat bran was carried out using the chemical activation method. $ZnCl_2$ was used as the chemical agent in the chemical activation. The impregnation ratio was used as 2:1, and the activation temperature was set to 500 °C. The activated carbon (WB-500) was used to remove the deep red dye substance from aqueous solutions. The outcome of the adsorption studies revealed that the highest adsorption capacity was attained when the adsorbent was exposed for 24 hours, maintained at a temperature of 45°C, and a pH of 2.17. The adsorption process effectively removed 95.238 mg with 1 g WB-500. Adsorption study was determined to follow the pseudo-second-order kinetic model and Langmuir isotherm. According to the second order, the adsorption rate increased from $1.22.10^{-4}$ to $3.43.10^{-4}$ with the increase in temperature from 25 °C to 45 °C. According to adsorption thermodynamics, adsorption is endothermic (ΔH^0, 41.08 kj mol^{-1}) and occurs physically and chemically forces. Activated carbon produced from wheat bran can effectively remove the Deep red dye substance from wastewater.

Keywords

Activated carbon,
Deep red,
Adsorption

Time Scale of Article

Received :07 February 2024
Accepted : 16 July 2024
Online date : 30 September 2024

1. INTRODUCTION

The dyes used in the textile industry's colouring fabrics, produced synthetically in different chemical structures and compositions, can reach the environment with wastewater and, from there, to living things [1]. The dyes used in the textile industry differ according to the type of fabric such as cotton dyes, dyes used for denim fabrics, fluorescent-coloured dyes, dyes used to dye linen and leather. Deep red (DR) (CAS:3564-22-5) belongs to the category of azo dyes, it is a synthetic organic compound that includes one or more azo groups (–N=N–).The structure of the DR is given in Figure 1. The presence of the azo group also plays a crucial role in the dyeing process, as it allows the dye to form strong covalent bonds with the substrate. The IUPAC name, Color Index (CI), molecular formula and molecular weight is (4Z)-4-[(4-methyll-2-nitrophenyl)hydrozinlidin]-N-(3-nitrophenyl)-3-oxynaphthalene-2-carboxyamide ,12350, $C_{24}H_{17}N_5O_6$, 471.42 g/mol, respectively [2]. Around 10,000 different textile colours are introduced to the market annually, and these dyes' wastewater is partially treated and discharged into the receiving waters. Therefore, dyes cause toxic, mutagenic and carcinogenic effects on aquatic animals

*Corresponding Author: caydin@ogu.edu.tr

and humans. Textile products are the product group that has the most relationship with the human body after foodstuffs. Paint residues and chemicals on our clothes penetrate our bodies through sweat and respiration and affect our health at least as much as the chemicals in foodstuffs. According to some studies, some of these chemicals cause allergies and carry a risk of cancer [3]. The limits of the amount of paint that can be found in wastewater in Turkey are determined by environmental legislation. The central legislations in Turkey include the Environmental Law [4], a regulation ensuring the prevention of water pollution to protect the potential of the country's underground and surface water resources and ensure their best use [5], the Wastewater Treatment Regulation and the Wastewater Discharge Regulation. According to these regulations, the amount of paint found in wastewater is determined depending on the type of paint and the area of use.

Single or hybrid processes are used to remove pollutants in water. There are various methods to purify water, such as reverse osmosis. This method operates by removing large molecules like dissolved salts and bacteria. Another method is Ion Exchange, which attracts different water ions to a solid surface with a charged structure. Beneficial ions are then released into the water [6,7]. Chemical precipitation is another water purification method [8]. Ultrafiltration and nanofiltration are used to purify water [9,10]. Flocculation, which is the process of forming aggregates of particles, is another method [11]. These methods have drawbacks, including high cost, maintenance, energy requirements, and management difficulties.

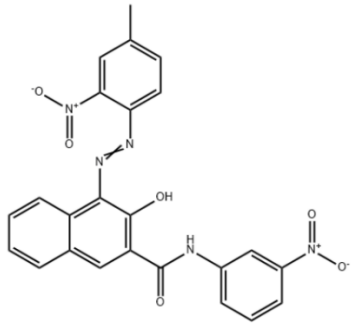

Figure 1. Molecular strucrure of deep red

Process; the equipment can be set up easily, and the hybrid systems can be easily adjusted to integrate with other treatment techniques. This method requires adsorbent material with a high affinity for contaminants. Adsorption is a technique known for its high effectiveness in removing pollutants from wastewater and ease of use. This approach has been widely utilized and has consistently yielded successful results [12]. Additionally, the adsorbent material can be regenerated through an appropriate desorption process, allowing it to be reused without losing its exceptional pollutant removal capabilities [13–15].

Activated carbon can retain various pollutants thanks to its porous structure with a surface area of 1800-2000 m^2 per gram. Due to its structure, it can selectively act as a sieve with different pore sizes and keep a wide variety of oxygenated functional groups bound on its surface. It can bind foreign substances on its surface and remove them from water. However, researchers continue to focus on the search for cheap raw materials to reduce production costs [16,17].

The consumption of naturally occurring biomass resources is a green method that has significant implications in many areas when used to derive functional porous carbons that are considered environmentally friendly, economical and sustainable [18]. Biomass is a renewable source of bio-organic-inorganic energy produced by natural and human-induced processes. The benefits of using biomass include easy processability, economic benefit and recyclability. The advantages of biomass over other carbon precursors are that it is naturally abundant, renewable, environmentally friendly and sustainable.

Examples of commonly used biomass include coconut shells [19], palm kernel shells [20], lotus stones [21], palm kernels [22], rise husk [23] leaves [24], sugarcane waste [25], rice husk [26], algae [27]. Renewable carbon sources such as glucose [28], chitin [29], chitosan [30], gelatin [31] and starch [32] can also be used as biopolymers. The characteristics of a carbon-based material, such as pore sizes, surface area, and grain size, can differ based on the raw biomass source. Additionally, the biomass source used can impact the quantity and variety of active sites on the material's surface. These active spots can capture a range of different types of molecules. The preparation of activated carbon from biomass consists of two main steps; first, the biomass is treated with a chemical agent. It is then carbonised in an oxygen-free environment and simultaneously improved by activating the microstructural properties of the carbon [33]. In this study, wheat bran was chosen as the starting material for synthesising the carbon-based adsorbent and the chemical activation method was used in the production process.

2. EXPERIMENTAL

2.1. Chemicals

Wheat bran (WB) was utilized as a carbon source, and Zinc chloride ($ZnCl_2$- reagent grade, ≥98%) served as the chemical activation agent in the chemical activation of WB. Sodium chloride (NaCl- ACS reagent, ≥99.0%) is employed in studies to determine the point of zero charge of active carbon. Hydrochloric acid (HCl- ACS reagent, 37%) and sodium hydroxide (NaOH- pellets for analysis EMSURE®) were employed to adjust the solutions to the desired pH.

2.2 Carbonisation Of Wheat Bran

In the synthesis of carbon-based adsorbents, chemicals are used to obtain a porous structure. Pre-treatment is carried out by impregnating the raw material in various proportions. For this purpose, wheat bran and $ZnCl_2$ were mixed. In a ratio of 2:1 by mass ($ZnCI_2$ g/raw material g), the chemical agent was mixed under a back cooler in a heated magnetic stirrer at 80 °C for 6 hours with 20 g of wheat bran. After the wheat bran absorbed the chemical, the filtration process was performed, and the soft and wet sample with cake structure was taken into drying containers and dried at 85 °C for 24 hours. The sample that had absorbed $ZnCl_2$ was then subjected to carbonisation. Remove some structures from the impregnated sample in Carbolite brand TZF 12/75/700 tube furnace at 500 °C for 1 hour in nitrogen atmosphere (100 $cm^3\,min^{-1}$ flow rate), starting from the laboratory temperature. After the sample was cooled, it was weighed and first washed in a 0.5 M hydrochloric acid (HCl), then filtered, and the sample, which was brought into contact with hot water repeatedly, was purified from the excess $ZnCl_2$ contained in it. The prepared sample was named WB-500.

2.3. Studies Of Deep Red Adsorption With WB-500

In the adsorption studies, the Thermo Electron AquaMete brand UV-vis spectrophotometer (UV-vis) device was used to determine the amount of deep red at 621 nm. A measure of the effectiveness of adsorbents is the magnitude of adsorption per gram of porous material. This is expressed in q_t (mg g^{-1}) and calculated using Eq.1. The percentage expression of the amount of deep red removed from the solution by adsorbing by the WB-500 was calculated by Eq.2.

$$q_t = \frac{(C_0 - C_t).V}{W} \tag{1}$$

$$Removal\ \% = \frac{(C_0 - C_e)}{C_0}.100 \tag{2}$$

C_0 (mg L^{-1}) is the amount of deep red contained in 1 litre of water before treatment; C_e (mg L^{-1}) is the amount of deep red in 1 litre of water after treatment. The concentration of deep red in the water during treatment is represented by C_t (mg L^{-1}); V is the volume of deep red solution used during treatment (L); W is the mass (g) of WB-500 brought into contact with contaminated water.

2.4. Determination of the Effect of the pH Value of Deep Red Solution

The pH_{PZC} value of the WB-500 sample was determined using the acid-base titration method. 0.1 g WB-500 and 50 ml of 0.02 M NaCl solution were placed in the conical flask and solutions were prepared with different pH values (pH_i). After 24 hours of agitation, the final pH values of the solutions were measured (pH_f). The $\Delta H=pH_f-pH_i$ value was graphed and the pH_{PZC} value was determined.

Necessary amounts of 0.1 M hydrochloric acid (HCl) or 0.1 M sodium hydroxide (NaOH) were added to the solutions to adjust the pH value of the deep red solution before treatment. For each experiment, 0.1 g of WB-500, 50 mL, 100 mg L^{-1} deep red solution were combined and placed in the flasks. The pH values of the solutions were adjusted with a pH meter to 2.14, 3.12, 4.06 (original), 5.04, 5.92, 7.14, 8.03 and 9.12. For 0.1 g of WB-500 remove the deep red in the solution by adsorption, the flasks were shaken in a water bath at 25°C for 24 hours.

2.5. Determination Of The Effect Of The Amount Of WB-500

For kinetics and isotherm studies, 50 mL of deep red water at 100 mg L^{-1} was used to determine the optimum amount of activated carbon. 0.025 g, 0.05 g, 0.1 g and 0.15 g WB-500 were contacted with polluted water at 25 °C in a shaking water bath heated at both initial pH (4.06) and pH 2.14 for 24 hours.

2.6. Kinetics And Equilibrium Experiments

In kinetic and equilibrium studies, 0.15 g WB-500 was brought into contact with 50 mL of deep red solution containing 100 mg L^{-1} deep red at a pH of 2.14. During the treatment process, kinetic studies were carried out at three different temperatures: 25, 35 and 45 °C. Non-adsorbed concentrations were measured by UV-vis, taking samples at regular intervals.

Equilibrium studies were conducted with solution containing different amounts of deep red (100, 150, 200, 250, 300, 350, 400 and 450 mg L^{-1}). In equilibrium studies, the initial pH of the solutions was adjusted to 2.14 and 0.15 g of WB-500 was used. The data obtained from equilibrium and kinetic studies were applied to the kinetic and isotherm models to understand the nature and mechanism of adsorption. All results were evaluated with an error of 5%. The results of the experiment were expressed in graphs using values calculated with 5% error. ($Yj=Yi\pm(Yi*0.05)$ where Yi is experimental results.) For the result obtained experimentally, two values are derived, taking 1.05 times and 0.95 times the experimental value. Using these two values, the error bar is plotted. This is done for each experimental outcome.

3. RESULTS

3.1. pH Effect

Activated carbon is an amphoteric solid because of the positive and negative groups that form the adsorption points attached to its surface. The zero point charge (pH_{PZC}) refers to the pH value where the net loads on the inner and outer surfaces of the porous material are zero. When the pH is bigger than pH_{PZC}, the activated carbon surface is negatively charged and suitable for adsorbing cations. When the pH is smaller than pH_{PZC}, the surface is positively charged and suitable for adsorbing anions [34]. Figure 2 shows the pH_{PZC} graph of deep red.

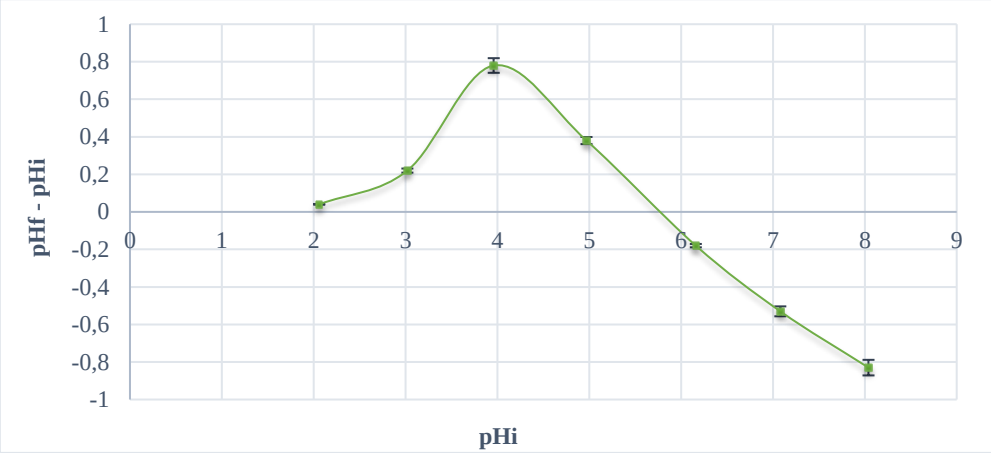

Figure 2. pH_{PZC} graph (WB-500: 0.1 g, V: 50 mL, C_0: 100 mg L^{-1}, T:25 °C, Time:24 h)

The value of the pH_{PZC} point is 5.9. The original pH of the deep red solution is about 4.06. In this case, when the pH value of the deep red solution is not changed without using any chemicals, the pH_{PZC} value is bigger than the pH value of the deep red solution. In water containing deep red, the surface of WB-500 is positively charged and tends to adsorb anions. In most adsorption studies, pH has been found to affect the adsorption process significantly [35]. Figure 3 shows the graph showing the effect of solution pH.

As a result of the studies carried out with deep red solutions with different pH values, WB-500 adsorbed 94% of the deep red in the solution at pH 2.14. As the pH value rises towards 9, the removal seems to decrease. This shows us that the adsorption capacity decreases at increasing pH values. It is observed that the removal does not change much between pH 4-6. Deep red dyestuff is a reactive dyestuff. The reactive end of the deep red dyestuff is negatively charged. Derici explained the high dark red removal at low pH values by replacing the hydrogen ions on the surface of the porous material with anionic dye molecules in the solution [36]. For this reason, the pH value was continued in the following studies by setting it to about 2.0. Derici et al. conducted studies on the adsorption of the Deep red dyestuff of activated carbon produced with kidney bean shells and reached the highest removal at pH 2 [36].

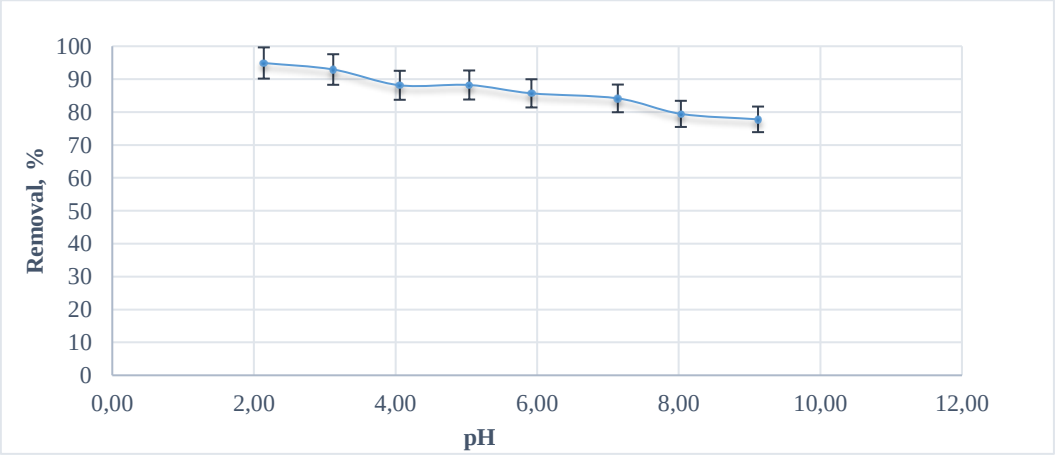

Figure 3. The effect of pH on deep red adsorption on WB-500 (WB-500: 0.1 g, V: 50 mL, C_0: 100 mg L^{-1}, T:25 °C, Time:24 h)

3.2. Effect of The Amount of WB-500

The increased amount of adsorbent leads to increased adsorption as it provides more adsorption centres, allowing more paint to be adsorbed to the surface [35]. In Figure 4, the % deep red adsorbed by different amounts of WB-500 at pH 2.14 and 4.06 and the amount of deep red removed per unit adsorbent are graphically expressed.

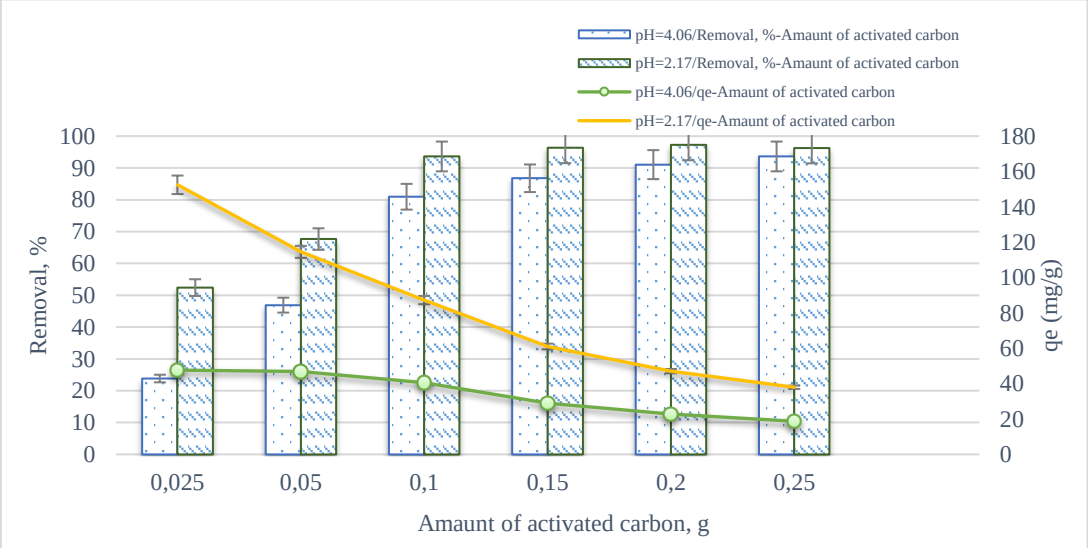

Figure 4. Amount of adsorbed Deep red per unit adsorbent in equilibrium against varying amounts of adsorbent and % amount of adsorption in equilibrium (V: 50 mL, C_0: 100 mg L^{-1}, T:25 °C, Time:24 h)

During dark red adsorption at pH 2.14, 0.05 g of WB-500 removed 67.65% of the dark red in the solution, while 0.15 g of WB-500 removed 96.33%.While the amount of WB-500 in contact with deep red increased to 0.20 g, WB-500 adsorbed 97.27% of the deep red in the solution. A similar change was observed at pH 4.06, and 0.15 g of WB-500 removed 86.76% of the deep red, and 0.20 g of WB-500 removed 91.05% of the deep red from the solution. As the amount of WB-500 in the solution increases, the probability of the adsorption active sites coming into contact with the deep red molecules increases. Thus, it is possible to remove more pollutants from the water. Using 0.15 g of WB-500 was appropriate in kinetic and balance studies. A slight increase in removal was observed when WB-500 increased from 0.15 g to 0.20 g at both pHs. In addition, since the increase in the amount of WB-500 is greater than the increase in the amount of adsorbed deep red, the qe value decreases. This shows that the increased amount of WB-500 will not be reflected in the amount of pollution removal from the water at the same rate.

3.3. Interaction Time

For this purpose, Figure 5 shows the change over time in the amount of deep red adsorbed by WB-500. Additionally, Figure 6 shows the graph showing the removal (%) amounts of deep red according to contact time. During the first 8 hours at all studied temperatures, deep red adsorption occurred rapidly, and the amount of adsorption increased continuously. At the end of 8 hours, 78.28% of deep red at 25 °C, 81.86% at 35 °C and 88.76% at 45 °C were removed from the aqueous solution. Since active sites of WB-500 in the solution were covered mainly with deep red molecules at the end of 8 hours, the increase in the amount of deep red adhered to the surface slowed down as the contact time increased. At all temperatures, adsorption reached equilibrium at 19 hours. After 19 hours, the active sites in the WB-500 absorbed 93.33 % of the dark red at 45°C.

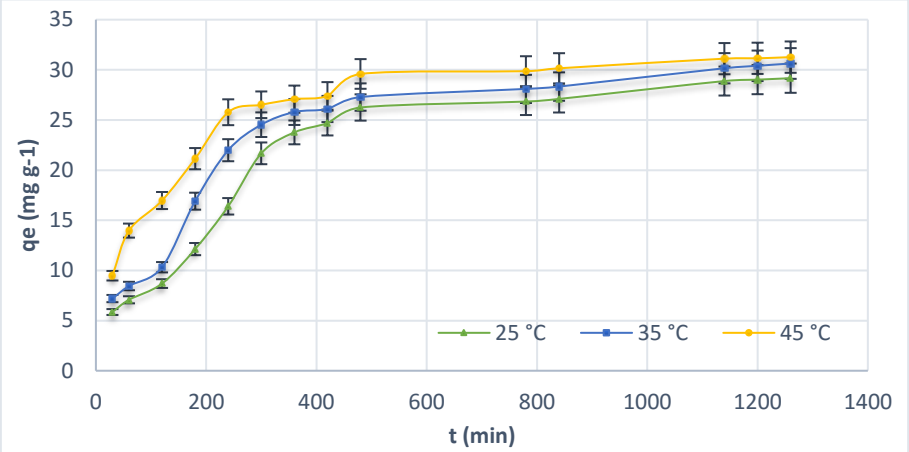

Figure 5. qe (mg g^{-1}) values against contact time (WB-500: 0.15 g, V: 50 mL, C_0: 100 mg L^{-1}, T: 25, 35 and 45 °C, pH: 2)

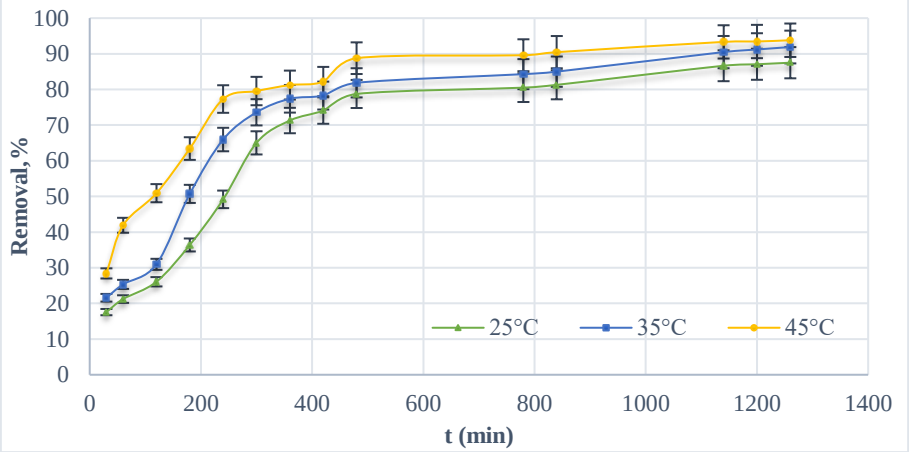

Figure 6. Deep red removal (%) values against contact time (WB-500: 0.15 g, V: 50 mL, C_0: 100 mg L^{-1}, T: 25, 35 and 45 °C, pH: 2)

The kinetic data obtained by using the amounts of dyes removed from the deep red property over time to examine the adsorption mechanism were applied to the Pseudo-First-Order (Pse. Fst. Or.) (Eq. (3) and Figure 7), Pseudo-Second-Order ((Pse. Sec. Or.)) (Eq. (4) and Figure 8) and Intra-Particle Diffusion kinetic models (Eq. (5) and Figure 9.). Table 1 gives the kinetic model parameters of deep red adsorption.

The pseudo-first-order :

$$\log(q_e - q_t) = log q_{e,1} - \frac{k_1 t}{2.303} \quad (3)$$

The pseudo-second-order:

$$\frac{t}{q_t} = \frac{1}{k_2 q_{e,2}^2} + \frac{t}{q_{e,2}} \quad (4)$$

Intra-particle diffusion model

$$q_t = k_i t^{0.5} + C \quad (5)$$

Where $q_{e,1}$ and $q_{e,2}$ are the maximum magnitude of the amount of adsorption per gram of WB-500 based on the pseudo-first-order kinetic model and pseudo-second-order kinetic model, respectively. k_1 is the first-order rate constant in units of $min^{-1,}$ and k_i is the intraparticle diffusion constant in units of mg g^{-1} $min^{-0.5}$. C is proportional to the boundary layer thickness, and k_2 is the pseudo-second-order rate constant in units of g mg^{-1} min^{-1} [37, 38].

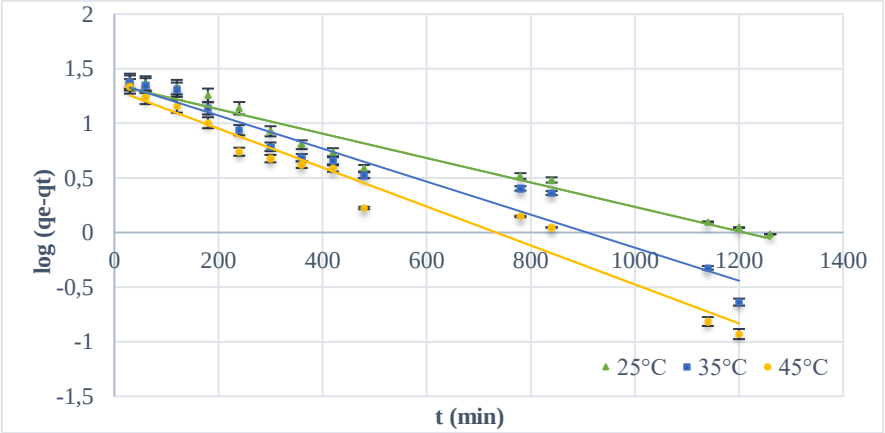

Figure 7. The PFO kinetic model of deep red adsorption.

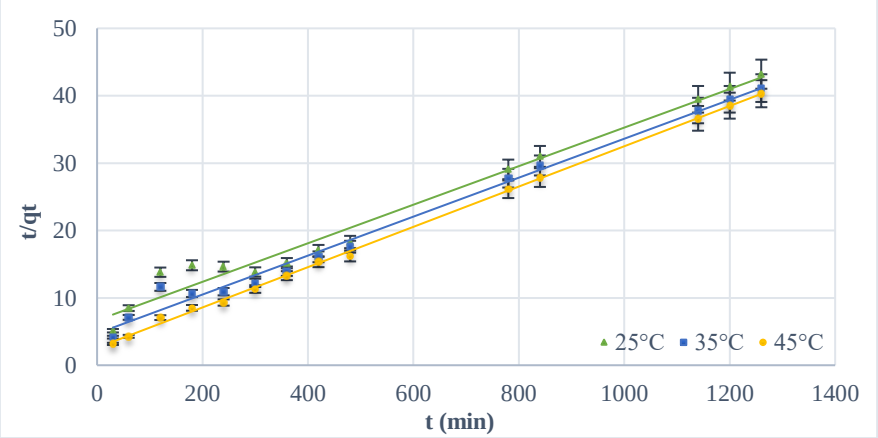

Figure 8. PSO kinetic model of deep red adsorption.

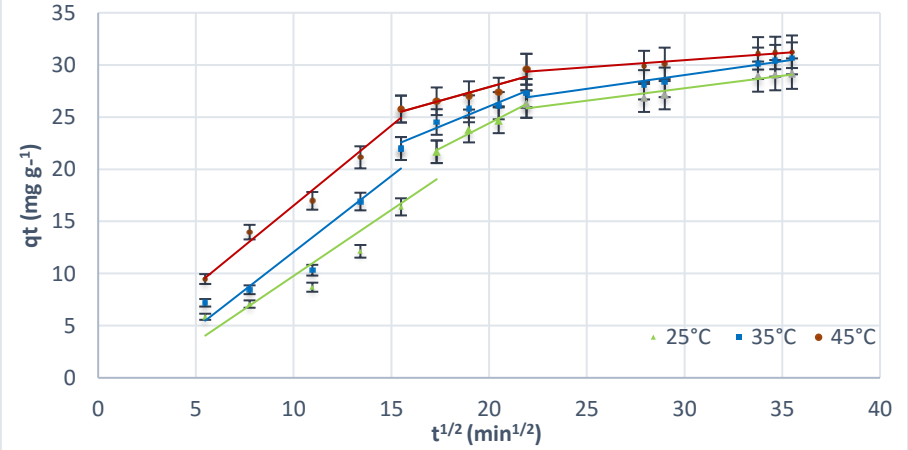

Figure 9. Intra-particle diffusion model of deep red adsorption.

Table 1. Kinetic model parameters of deep red adsorption.

First-order kinetic model			
	25 °C	**35 °C**	**45 °C**
$q_{e,1}$(mg g^{-1})	22.53	23.64	20.33
k_1 (min^{-1})	$2.53.10^{-3}$	$3.45.10^{-3}$	$4.14.10^{-3}$
R^2	0.95	0.94	0.96
Second-order kinetic model			
	25 °C	**35 °C**	**45 °C**
$q_{e,2}$ (mg g^{-1})	34.96	34.60	33.44
k_2 (g $mg^{-1}.min^{-1}$)	$1.22.10^{-4}$	$1.77.10^{-4}$	$3.43.10^{-4}$
R^2	0.97	0.99	0.99
Intra-particle diffusion model			
	25 °C	**35 °C**	**45 °C**
k_{id} (mg g^{-1} $min^{-0.5}$)	0.96	0.77	0.52
C	5.21	10.66	17.39
R^2	0.98	0.93	0.85

They were comparing the Pse. Sec. Or. kinetic and Pse. Ft. Or. kinetic models, the Pse. Sec. Or. kinetic model better represents the kinetic data based on the time that WB-500 removes deep red by adsorption in all three temperatures. The rate constants of the Pse. Sec. Or. kinetic model shows that the reaction occurs slowly and that the adsorption rate increases with the increase in temperature. The experimental value of q_e is 30.12 mg g^{-1}.

The shape of the graph of the intraparticle diffusion model can give information about the adsorption mechanism. Suppose the deep red molecules attached to the WB-500 surface reach the pores or the surface by film diffusion due to the water covering the WB-500 surface. In that case, the graph consists of 3 parts, and the graph does not pass through the origin and has a C value. The graph's second part is formed if the deep red molecules reach the adsorption points by intraparticle diffusion and advance in the activated carbon's pores. The third part of the graph represents the adsorption step. [39]. The intra-particle diffusion pattern appears to occur in three phases. This shows us that the adsorption process takes place gradually. The k_{id} value is decreased from 0.96 mg g^{-1} $min^{-0.5}$ to 0.52 mg g^{-1} $min^{-0.5}$. As the temperature increased, the effect of film diffusion on adsorption increased, while the effect of intra-particle diffusion decreased. The temperature increase increased the C value from 5.21 to 17.39. This shows us that the temperature increase causes the film layer thickness, where film diffusion occurs, to increase.

3.4. Equilibrium Experiments

How molecules or ions interact with the solid surface can be explained by adsorption isotherms that provide information about the equilibrium states of an adsorption system. The main objective in expressing the data obtained during the adsorption process of the dye molecules of different initial concentrations with isotherms is to show the equilibrium conditions of the porous material and porous material relationship and to reveal the deposition mechanism of the substances on the surface [40]. Equilibrium data of the adsorption of deep red were obtained by performing experiments in deep red solutions at 3 different temperatures and different initial concentrations, and the data are presented in Figure 10. The conformity of the obtained data to four different isotherms was examined. Linear forms of isotherms are given in Eq. (6-9). The Langmuir isotherm model describes adsorbed molecules on a homogeneous surface containing adsorption points with similar attractive forces and in which the molecules are adsorbed in a single layer. At the same time, according to the Langmuir model, all active sites are considered to have the same energy and equal interest in the molecules to be adsorbed. The

isotherm plots and constants of deep red adsorption are given in Figure 11 and Table 2, respectively. [35,41].

Langmuir

$$q_e = \frac{q_L K_L C_e}{1 + K_L C_e} \qquad \frac{C_e}{q_e} = \frac{1}{q_L K_L} + \frac{C_e}{q_L} \tag{6}$$

Freundlich

$$q_e = K_F C_e^{1/n} \qquad \log(q_e) = \log K_F + \frac{1}{n}\log C_e \tag{7}$$

Temkin

$$q_e = \frac{RT}{b_T} ln(K_T C_e) \qquad q_e = B_1\, lnK_T + B_1\, lnC_e \tag{8}$$

Dubinin–Radushkevich (D–R)

$$lnq_e = lnq_m - \beta\varepsilon^2 \tag{9}$$

- q_L: Langmuir adsorption capacity of the WB-500 (mg g^{-1})
- K_L: Langmuir adsorption constant (dm^3 mg^{-1})
- K_F and n are Freundlich constants
- b_T: Temkin constant (j mol^{-1})
- K_T: The equilibrium binding constant (L g^{-1})
- q_m: Theoretical monolayer saturation capacity (mg g^{-1})
- ε, The Polanyi potential, $\varepsilon = RTln(1 - 1/C_e)$
- T: Temperature (K)
- R: The universal gas constant (8,314 J $mol^{-1}K^{-1}$)
- β: Dubinin–Radushkevich constant (mol^2 J^{-2})
- E: The average free energy of adsorption (kJ mol^{-1}), $E = \frac{1}{(2\beta)^{1/2}}$

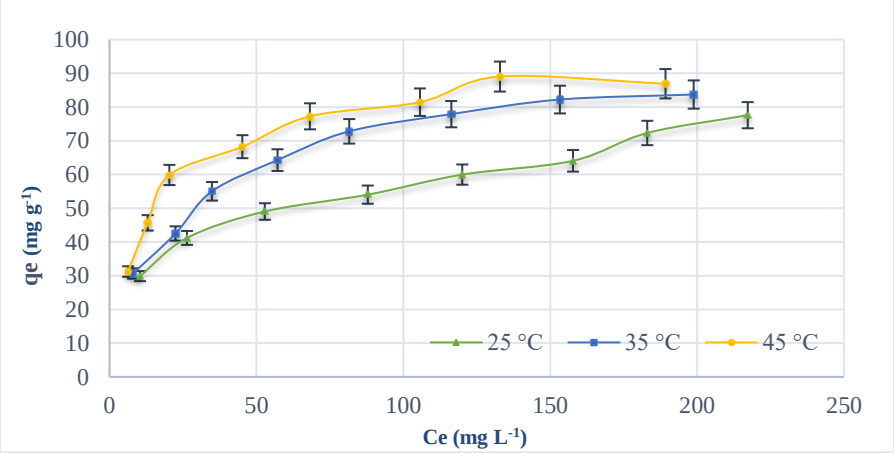

Figure 10. The effect of temperature on deep red adsorption. (WB-500: 0.15 g, V: 50 mL, T: 25, 35 and 45 °C, Time: 24 h, pH: 2)

There is a relationship of qe (45 °C) > qe (35 °C) > qe (25 °C) between the qe values obtained in all studies performed in deep red solutions with different initial concentrations. The temperature increase positively affected the adsorption capacity of WB-500 under equilibrium conditions. The adsorption nature of deep red is thermodynamically endothermic.

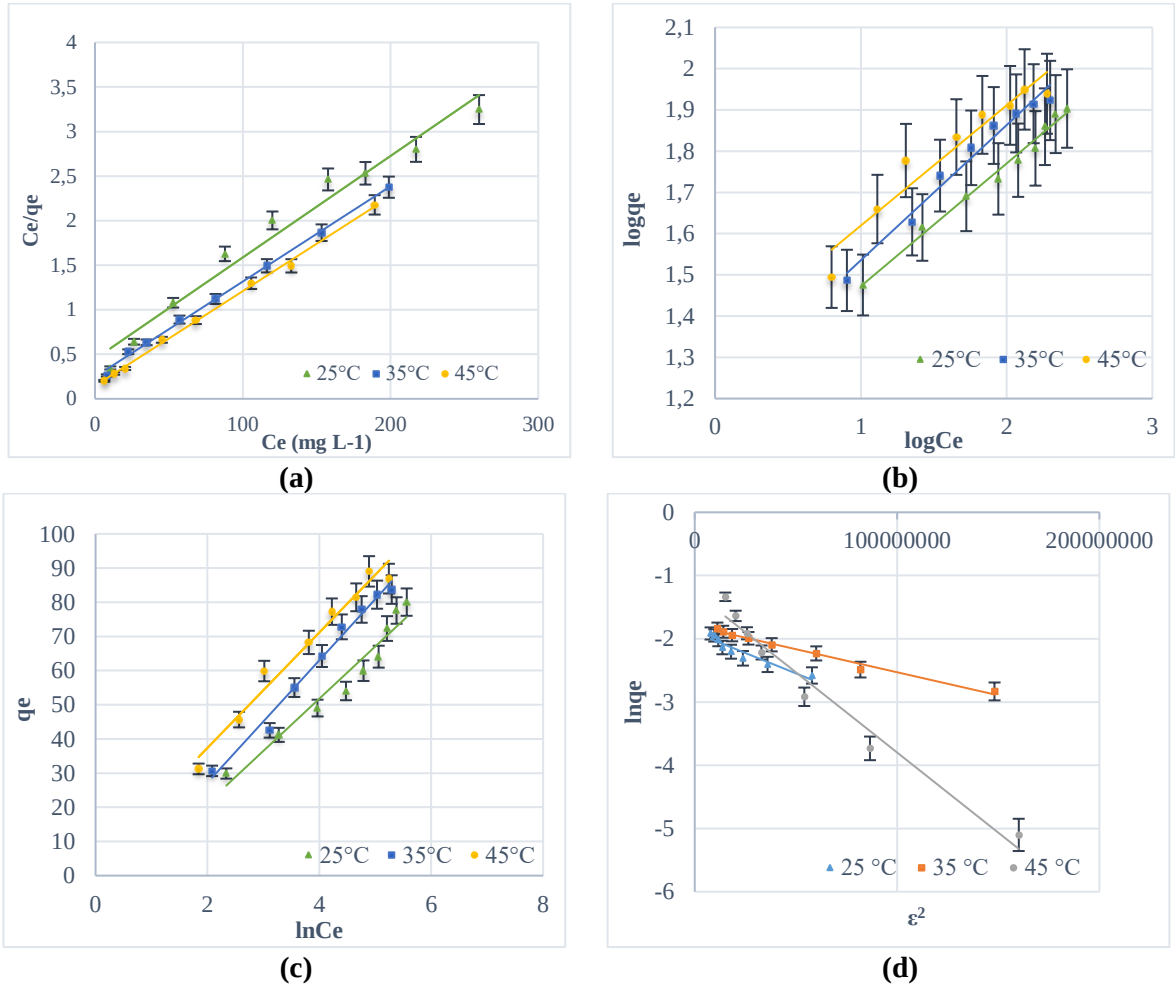

Figure 11. Isotherm models' graphs Langmuir (a), Freundlich (b), Temkin (c) and The Dubinin– Radushkevich (D–R) (d)

When the isotherm graphs drawn using data obtained from studies conducted at different temperatures were compared, the experimental data in the Freundlich model deviated from the model line. Due to the homogeneity of WB-500 produced from wheat bran, the adsorbing behaviour of deep red is suitable for the Langmuir type. The 1/n values are close to zero, and the surface of the activated carbon is homogeneous.

Deep red's maximum monolayer adsorption capacities were calculated according to the Langmuir model in Table 2. The q_L values for 25, 35 and 45 °C are 87.71, 93.45 and 95.23 mg g^{-1}, respectively. As can be seen, the Langmuir adsorption capacities increased as the temperature increased. The Temkin model is the adsorption isotherm, which considers the interactions between adsorbed substances. The Temkin equation states that as the adsorbed molecules adhere to the surface of the porous material, the active adsorption points decrease, and a linear decrease in the adsorption energy occurs [42]. According to the Temkin isotherm equation, the heat of adsorption at 25 °C is obtained as 162.12 j mol^{-1}, while for 45 °C, it is obtained as 156.7 j $mol^{-1.}$ As the temperature increased, the amount of coating of the adsorbed increased, and therefore the adsorption heat decreased.

The Dubinin–Radushkevich model is more general than the Langmuir model. The Dubinin-Radushkevich model does not assume that adsorption occurs on a homogeneous surface. The E value explains whether the adsorption mechanism occurs by the ion exchange mechanism or by the effect of

van der Waals forces [39]. According to the D-R model, one mole of deep red is adsorbed to the active points of WB-500 at 25, 35 and 45 °C with an adsorption energy of 7.07, 8.45 and 4.08 kj, respectively. Since these values are close to 8 kj and less than 8 kj, the deep red molecules may have been held onto the surface by van der Waals forces.

Table 2. Isotherm model parameters of deep red adsorption.

Langmuir Isotherm model			
	q_L (mg g^{-1})	**K_L (L mg^{-1})**	**R^2**
25 °C	87.71	0.025	0.97
35 °C	93.45	0.043	0.99
45 °C	95.23	0.072	0.99
Freundlich Isotherm model			
	1/n	**K_f**	**R^2**
25 °C	0.30	3.23	0.98
35 °C	0.33	3.34	0.97
45 °C	0.29	3.77	0.92
Temkin Isotherm model			
	b_T	**K_T**	**R^2**
25 °C	162.12	0.54	0.94
35 °C	143.2	0.61	0.98
45 °C	156.7	1.23	0.97
The Dubinin–Radushkevich (D–R) Isotherm model			
	E (kj mol^{-1})	**q_m (mg g^{-1})**	**R^2**
25 °C	7.07	81.19	0.89
35 °C	8.45	89.85	0.98
45 °C	4.08	153.74	0.96

3.5. Adsorption Thermodynamics

Gibbs free energy (Eq.10), entropy and enthalpy parameters were examined to examine the thermodynamics of studies with deep red adsorption. Using the K_L values obtained from the Langmuir equation, the $\ln K_L$ values against 1/T were graphed and given in Figure 12 The thermodynamic values of ΔH^o and ΔS^o were calculated by Eq. 11.

$$\Delta G^{\,0} = -RTlnK_L \tag{10}$$

$$\Delta G^o = \Delta H^0 - T\Delta S^0 \tag{11}$$

The free energy change (ΔG^o) in the adsorption of dark red was calculated to be approximately -23.28, -25.43 and -27.59 kj mol^{-1} at 25, 35 and 45 °C. Generally, the change of free energy for physisorption is between -20 and 0 kJ mol^{-1}, the physisorption together with chemisorption is at the range of -20 to -80 kJ mol^{-1} and chemisorption is at a range of -80 to -400 kJ mol^{-1} [43]. According to the free energy exchange results, the adsorption process occurred under the influence of physical and chemical forces [44]. ΔH^o value of 41.08 kj mol^{-1} indicates the system must receive heat for adsorption. The ΔS^o value was calculated as 215.86 j mol^{-1} K^{-1}, and the positive value of entropy indicates an increase in randomness and irregularity at the solid/solution interface. This indicates that adsorption occurs with increased entropy [45,46].

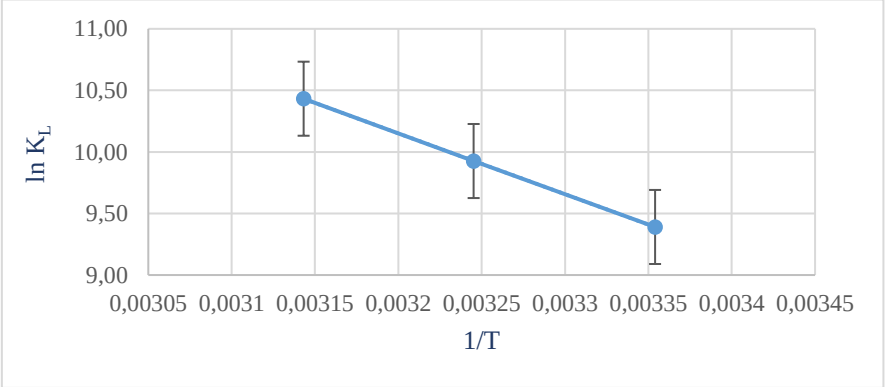

Figure 12. 1/T versus lnK_L exchange of deep red adsorption.

4. CONCLUSIONS

In this study, wheat bran was recycled, and activated carbon production with economic value was realised. The deep red adsorption capacity of the activated carbon produced was determined. The nature of adsorption was determined by performing kinetic and equilibrium studies. Deep red's maximum monolayer adsorption capacities were calculated according to the Langmuir model as are 87.71, 93.45 and 95.23 mg g^{-1} for 25, 35 and 45 °C, respectively. Based on the Temkin isotherm, as temperature increased, the quantity of adsorbed coating rose, leading to a decrease in the heat of adsorption 162.12 j mol^{-1} to 156.7 j mol^{-1}. According to the results of the kinetic study, deep red adsorption on WB-500 increased from $1.22.10^{-4}$ to $3.43.10^{-4}$ g $mg^{-1}.min^{-1}$ as the temperature dropped from 25 °C to 45 °C. The adsorption process takes place gradually according to the intra-particle diffusion modal. The k_{id} value is decreased from 0.96 mg g^{-1} $min^{-0.5}$ to 0.52 mg g^{-1} $min^{-0.5}$. The Langmuir model has a better correlation coefficient than other mathematical models at all temperatures examined in the current study. The resulting single-layer adsorption capacity value was obtained at 95.23 mg g^{-1} 45 °C. In conclusion, the results show that activated carbon produced from wheat bran can be effectively applied to remove deep red from wastewater.

CONFLICT OF INTEREST

The authors declare that they have no conflict of interest regarding the publication of this article.

ACKNOWLEDGMENTS: This study was prepared within the scope of the Master's Thesis studies conducted by Fatma Betül Kuş, a student of Eskişehir Osmangazi University, Institute of Natural and Applied Sciences, Department of Chemical Engineering.

CRediT AUTHOR STATEMENT:

Ilknur Demiral: Conceptualization, Data curation, Formal Analysis, Investigation, Methodology, Resources, Supervision, Review and editing. **Canan Samdan:** Conceptualization, Data curation, Formal Analysis, Investigation, Methodology, Supervision, Visualization, Writing – original draft & editing, **Fatma Betül Kus:** Conceptualization, Data Curation, Formal Analysis, Methodology, Validation, Writing

REFERENCES

[1] Schneider K, Hafner C, Jäger I. Mutagenicity of textile dye products. J Appl Toxicol. 2004; 24 (2), 83-91.

[2] Deep Red Cas#: 3564-22-5. ChemicalBook. https://m.chemicalbook.com/Product ChemicalProperties CB8356989_EN.htm. Accessed May 29, 2024.

[3] Sulistina DR, Martini S. The Effect of Rhodamine B on the Cerebellum and Brainstem Tissue of Rattus Norvegicus. J Public Health Res. 2020; 9 (2).

[4] Environmental Law. 1983. https://www.mevzuat.gov.tr/MevzuatMetin/1.5.2872.pdf. Accessed June 22, 2023.

[5] Water Pollution Control Regulation.; 2004:25687. https://www.mevzuat.gov.tr/mevzuat?MevzuatNo=7221&MevzuatTur=7&MevzuatTertip=5. Accessed June 22, 2023.

[6] Inamuddin. Applications of Adsorption and Ion Exchange Chromatography in Waste Water Treatment. Materials Research Forum LLC, 2017.

[7] Wong CW, Barford JP, Chen G, McKay G. Kinetics and equilibrium studies for the removal of cadmium ions by ion exchange resin. J Environ Chem Eng. 2014; 2 (1), 698-707.

[8] Zamora-Ledezma C, Negrete-Bolagay D, Figueroa F, Zamora-Ledezma E, Ni M, Alexis F, et al. Heavy metal water pollution: A fresh look about hazards, novel and conventional remediation methods. Environ Technol Innov. 2021; 22, 101504.

[9] Secondes MFN, Naddeo V, Belgiorno V, Ballesteros F. Removal of emerging contaminants by simultaneous application of membrane ultrafiltration, activated carbon adsorption, and ultrasound irradiation. J Hazard Mater. 2014; 264, 342-349.

[10] Abdel-Fatah MA. Nanofiltration systems and applications in wastewater treatment: Review article. Ain Shams Eng J. 2018;9 (4), 3077-3092.

[11] Teh CY, Budiman PM, Shak KPY, Wu TY. Recent Advancement of Coagulation–Flocculation and Its Application in Wastewater Treatment. Ind Eng Chem Res. 2016; 55 (16), 4363-4389.

[12] Savci S, Donmez S, Mazmanci MA. Performance And Mechanısms Of Malachıte Green Dye Adsorptıon Usıng Industrıal Solıd Waste As Adsorbent. Environ Eng Manag J. 2023; 22 (1), 97-104.

[13] Simsek R, Ciftci BN, Uysal Y. An Experımental Study On The Effıcıency Of Chromıum (VI) Removal Wıth Starch-Magnetıte Nanocomposıte (Starch@Mnps). Anadolu Univ J Sci Technol-Appl Sci Eng. 2020; 21 (2), 322-334.

[14] Dikmen S, Ersoy B, Dikmen Z. Adsorptıon Behavıour Of Ionıc And Non-Ionıc Surfactants Onto Talc A Naturally Hydrophobıc Mıneral-A Comparatıve Study. Eskişehir Tech Univ J Sci Technol - Appl Sci Eng. 2020; 21 (1), 139-152.

[15] Savci S, Uysal MM. Adsorption of Methylene Blue and Methyl Orange By Using Waste Ash. Süleyman Demirel Üniversitesi Fen Bilim Enstitüsü Derg. 2017; 21 (3), 831.

[16] Neolaka YAB, Riwu AAP, Aigbe UO, Ukhurebor KE, Onyancha RB, Darmokoesoemo H, et al. Potential of activated carbon from various sources as a low-cost adsorbent to remove heavy metals and synthetic dyes. Results Chem. 2023; 5, 100711.

[17] Başar B, Şayan E. Optımızatıon Of Selectıve Cu^{2+} Adsorptıon Wıthın The Multı-Ion System By Usıng Actıvated Carbon Prepared By Ultrasound. Anadolu Univ J Sci Technol- Appl Sci Eng. 2018; 19 (4), 893-906.

[18] Manasa P, Sambasivam S, Ran F. Recent progress on biomass waste derived activated carbon electrode materials for supercapacitors applications—A review. J Energy Storage. 2022; 54, 105290.

[19] Yağmur HK, Kaya İ. Synthesis and characterization of magnetic $ZnCl_2$-activated carbon produced from coconut shell for the adsorption of methylene blue. J Mol Struct. 2021; 1232, 130071.

[20] Syed-Hassan SSA, Zaini MSM. Optimization of the preparation of activated carbon from palm kernel shell for methane adsorption using Taguchi orthogonal array design. Korean J Chem Eng. 2016; 33 (8), 2502-2512.

[21] Boudechiche N, Fares M, Ouyahia S, Yazid H, Trari M, Sadaoui Z. Comparative study on removal of two basic dyes in aqueous medium by adsorption using activated carbon from Ziziphus lotus stones. Microchem J. 2019; 146, 1010-1018.

[22] Kundu A, Sen Gupta B, Hashim MA, Redzwan G. Taguchi optimization approach for production of activated carbon from phosphoric acid impregnated palm kernel shell by microwave heating. J Clean Prod. 2015; 105, 420-427.

[23] Metin N, Savci S. Adsorption of Malachite Green by An Agricultural Waste: Rice Husk. Türk Tarım Ve Doğa Bilim Derg. 2021; 8 (1), 23-29.

[24] Mosoarca G, Vancea C, Popa S, Gheju M, Boran S. Syringa vulgaris leaves powder a novel low-cost adsorbent for methylene blue removal: isotherms, kinetics, thermodynamic and optimization by Taguchi method. Sci Rep. 2020; 10 (1), 17676.

[25] Srenscek-Nazzal J, Kamińska W, Michalkiewicz B, Koren ZC. Production, characterization and methane storage potential of KOH-activated carbon from sugarcane molasses. Ind Crops Prod. 2013; 47, 153-159.

[26] Luo Y, Li D, Chen Y, Sun X, Cao Q, Liu X. The performance of phosphoric acid in the preparation of activated carbon-containing phosphorus species from rice husk residue. J Mater Sci. 2019; 54 (6), 5008-5021.

[27] Aravindhan R, Raghava Rao J, Unni Nair B. Preparation and characterization of activated carbon from marine macro-algal biomass. J Hazard Mater. 2009; 162 (2-3), 688-694.

[28] Eshghi A, kheirmand M. Graphene/Ni–Fe layered double hydroxide nano composites as advanced electrode materials for glucose electro oxidation. Int J Hydrog Energy. 2017; 42 (22), 15064-15072.

[29] Das MP. Removal of Methylene Blue by Adsorption Using Fish Scale Chitin. Nat Environ Pollut Technol. 2018; 17 (3), 7.

[30] Wong KT, Wong VL, Lim SS. Bio-sorptive Removal of Methyl Orange by Micro-Grooved Chitosan (GCS) Beads: Optimization of Process Variables Using Taguchi L9 Orthogonal Array. J Polym Environ. 2021; 29 (1), 271-290.

[31] Mahmoud ME. Water treatment of hexavalent chromium by gelatin-impregnated-yeast (Gel–Yst) biosorbent. J Environ Manage. 2015; 147, 264-270.

[32] Chen L, Zhu Y, Cui Y, Dai R, Shan Z, Chen H. Fabrication of starch-based high-performance adsorptive hydrogels using a novel effective pretreatment and adsorption for cationic methylene blue dye: Behavior and mechanism. Chem Eng J. 2021; 405, 126953.

[33] Malini K, Selvakumar D, Kumar NS. Activated carbon from biomass: Preparation, factors improving basicity and surface properties for enhanced CO_2 capture capacity – A review. J CO_2 Util. 2023; 67, 102318.

[34] Zhang Y, Song X, Xu Y, Shen H, Kong X, Xu H. Utilization of wheat bran for producing activated carbon with high specific surface area via NaOH activation using industrial furnace. J Clean Prod. 2019; 210, 366-375.

[35] Alomar T, Qiblawey H, Almomani F, Al-Raoush RI, Han DS, Ahmad NM. Recent advances on humic acid removal from wastewater using adsorption process. J Water Process Eng. 2023; 53, 103679.

[36] Derici C. Production of Activated Carbon from Kidney Bean Shells and Its Use in Dyestuff Removal. Master Thesis. Eskişehir Osmangazi University Institute of Science and Technology, 2021.

[37] Khaled A, El Nemr A, El-Sikaily A, Abdelwahab O. Treatment of artificial textile dye effluent containing Direct Yellow 12 by orange peel carbon. Desalination. 2009; 238 (1), 210-232.

[38] Torres-Perez J, Gerente C, Andres Y. Conversion of agricultural residues into activated carbons for water purification: Application to arsenate removal. J Environ Sci Health Part A. 2012; 47 (8), 1173-1185.

[39] Hydari S, Sharififard H, Nabavinia M, Parvizi MR. A comparative investigation on removal performances of commercial activated carbon, chitosan biosorbent and chitosan/activated carbon composite for cadmium. Chem Eng J. 2012; 193-194.

[40] Garg V. Basic dye (methylene blue) removal from simulated wastewater by adsorption using Indian Rosewood sawdust: a timber industry waste. Dyes Pigments. 2004; 63 (3), 243-250.

[41] Naghizadeh A, Momeni F, Kamani H. Study of Ultrasonic Regeneration and Adsorption of Humic Acid on Activated Carbon. Health Scope. 2018; 7 (2).

[42] Danish M, Ahmad T, Majeed S, Ahmad M, Ziyang L, Pin Z, et al. Use of banana trunk waste as activated carbon in scavenging methylene blue dye: Kinetic, thermodynamic, and isotherm studies. Bioresour Technol Rep. 2018; 3, 127-137.

[43] Gerçel Ö, Özcan A, Özcan AS, Gerçel HF. Preparation of activated carbon from a renewable bio-plant of Euphorbia rigida by H_2SO_4 activation and its adsorption behavior in aqueous solutions. Appl Surf Sci. 2007; 253 (11), 4843-4852.

[44] Mei D, Liu L, Yan B. Adsorption of uranium (VI) by metal-organic frameworks and covalent-organic frameworks from water. Coord Chem Rev. 2023; 475, 214917.

[45] Benjelloun M, Miyah Y, Akdemir Evrendilek G, Zerrouq F, Lairini S. Recent Advances in Adsorption Kinetic Models: Their Application to Dye Types. Arab J Chem. 2021; 14 (4), 103031.

[46] Chen S, Qin C, Wang T, Chen F, Li X, Hou H, et al. Study on the adsorption of dyestuffs with different properties by sludge-rice husk biochar: Adsorption capacity, isotherm, kinetic, thermodynamics and mechanism. J Mol Liq. 2019; 285, 62-74.